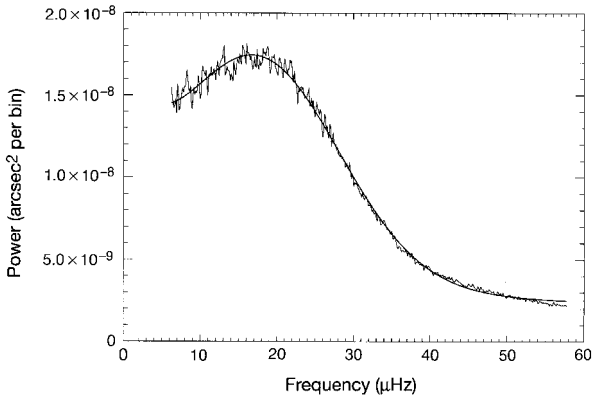

Figure 5 The mean power spectrum averaged over solar latitude. This was computed by assuming that the limb power spectra are due to a photospheric displacement pattern, rotating across the limb at various velocities corresponding to the local latitudinal rotation speed. The mean spectrum is obtained by first stretching the frequency scale of each latitudinal spectrum to match the equatorial spectrum (by linear interpolation onto the new frequency domain), and then averaging these on the common frequency domain. A simple shift of each spectrum by a frequency equal to the sawtooth variation with latitude (from Fig. 4) also matches the broad power excess at each latitude to the equatorial rate, yielding a mean spectrum which is essentially the same as the scaled frequency result displayed here. The solid line shows a least-squares fit to a gaussian and a power-law background distribution. The resulting centre frequency is 18 μHz.

timeseries (over many characteristic timescales) will the power spectrum yield a peak at the average temporal frequency. Thus, a test of the stochastic or supergranule hypothesis requires looking for a lorentzian form to the low-frequency spectrum.

The spectrum from a single latitude bin is too noisy to distinguish a monotonic excess power signal (a lorentzian) from the generally increasing displacement noise power towards lower frequencies. Combining spectra from a range of latitude bins improves the signal-to-noise ratio. We find a gaussian peak in the mean spectrum (Fig. 5) with a centre frequency of 18 μHz. The existence of a spectral peak suggests that at least a portion of the low-frequency power is not caused by supergranules. Although the spectrum also contains a displacement 'background' signal which increases to lower frequencies, the peak signal (corresponding to a 15-h period) is best described as a low-Q oscillator. It has long-range order and is not a stochastic 'random telegraph'. A standing wave is a natural mechanism for producing such a lattice of solar 'hills'. Wolff[13,14] previously suggested that a large-scale photospheric nodal pattern generated by phase-locked r-modes would evolve over timescales of a few days—a result in qualitative agreement with the low-Q oscillator we see here in the mean limb displacement power spectrum. If r-modes are driven by the largest scales of convection, we should also expect a characteristic length scale of the order of the depth of the convection zone: that is, 2×10^5 km. The transverse scale we observe is half this, but is plausibly consistent.

The magnitude of the vertical displacement is also energetically reasonable. If subphotospheric convection is spatially organized by Rossby modes, then even velocities of 100 m s^{-1} (a small fraction of measured photospheric convective velocities) are energetic enough to lift up the overlying photosphere by the observed 100-m vertical height. Although it remains to be seen from detailed model calculations exactly how global solar r-modes could be excited, the existence of a corrugated photosphere with long-range order is good evidence for these oscillations. □

Received 16 December 1999; accepted 16 March 2000.

1. Plaskett, H. H. The polar rotation of the Sun. *Mon. Not. R. Astron. Soc.* **131,** 407–433 (1966).
2. Chelton, D. B. & Schlax, M. G. Global observations of oceanic Rossby waves. *Science* **272,** 234–238 (1996).
3. Wolff, C. L. Linear r-mode oscillations in a differentially rotating star. *Astrophys. J.* **502,** 961–967 (1998).
4. Papaloizou, J. & Pringle, J. E. Non-radial oscillations of rotating stars and their relevance to the short-period oscillations of cataclysmic variables. *Mon. Not. R. Astron. Soc.* **182,** 423–442 (1978).
5. Kumar, P., Quataert, E. & Bahcall, J. Observational searches for solar g-modes: some theoretical considerations. *Astrophys. J.* **458,** 83–L85 (1996).
6. Provost, J., Berthomeiu, G. & Rocca, A. Low frequency oscillations of a slowly rotating star—quasi toroidal modes. *Astron. Astrophys.* **94,** 126–133 (1981).
7. Wolff, C. L. & Blizard, J. B. Properties of r-modes in the Sun. *Sol. Phys.* **105,** 1–15 (1986).
8. Kuhn, J. R., Bush, R., Scheick, X. & Scherrer, P. The Sun's shape and brightness. *Nature* **392,** 155–157 (1998).
9. Lazrek, M. *et al.* First results on p-modes from GOLF experiment. *Sol. Phys.* **175**, 227–246 (1997).
10. Scherrer, P. H. *et al.* The solar oscillations investigation—Michelson Doppler Imager. *Sol. Phys.* **162,** 129–188 (1995).
11. Schrijver, C. J., Hagenaar, H. R. & Title, A. M. On the patterns of the solar granulation and supergranulation. *Astrophys. J.* **475,** 328–337 (1997).
12. Rice, S. O. Mathematical analysis of random noise. *Bell Syst. Tech. J.* **23,** 1–162 (1944).
13. Wolff, C. L. Distinctive patterns on the surface of slowly rotating stars whose oscillations are non-linearly coupled. *Astrophys. J.* **193,** 721–727 (1974).
14. Wolff, C. Oscillation convection coupling: cause of supergranulation. *Astrophys. J.* **443,** 423–433 (1995).

Acknowledgements

We thank J. Saba, C. DeForest and J. Covington for assistance in operating the MDI instrument during these observations. We are particularly grateful to R. Bogart and to X. Scheick for their help with the limb software analysis.

Correspondence and requests for materials should be addressed to J.R.K. (e-mail: jkuhn@solar.stanford.edn).

Acceleration of quantum decay processes by frequent observations

A. G. Kofman & G. Kurizki

Department of Chemical Physics, The Weizmann Institute of Science, Rehovot 76100, Israel

In theory, the decay of any unstable quantum state can be inhibited by sufficiently frequent measurements—the quantum Zeno effect[1–10]. Although this prediction has been tested only for transitions between two coupled, essentially stable states[5–8], the quantum Zeno effect is thought to be a general feature of quantum mechanics, applicable to radioactive[3] or radiative decay processes[6,9]. This generality arises from the assumption that, in principle, successive observations can be made at time intervals too short for the system to change appreciably[1–4]. Here we show not only that the quantum Zeno effect is fundamentally unattainable in radiative or radioactive decay (because the required measurement rates would cause the system to disintegrate), but also that these processes may be accelerated by frequent measurements. We find that the modification of the decay process is determined by the energy spread incurred by the measurements (as a result of the time–energy uncertainty relation), and the distribution of states to which the decaying state is coupled. Whereas the inhibitory quantum Zeno effect may be feasible in a limited class of systems, the opposite effect—accelerated decay—appears to be much more ubiquitous.

We recall the common argument leading to the quantum Zeno effect (QZE)[3,4]. If a system ruled by hamiltonian $\hat{H}$ is in state $|e\rangle$ at $t = 0$, the probability to find the system there at $t > 0$ is:

$$\rho_{ee}(t) = \left| \left\langle e \left| \exp\left(-\frac{i}{\hbar}\hat{H}t \right) \right| e \right\rangle \right|^2 \qquad (1)$$

Provided the hamiltonian variance $\langle V^2\rangle = \langle e|\hat{H}^2|e\rangle - \langle e|\hat{H}|e\rangle^2$ is finite, then, at short times $\langle V^2\rangle t^2/\hbar^2 \ll 1$:

$$\rho_{ee}(t) \approx 1 - \langle V^2\rangle t^2/\hbar^2 \tag{2}$$

If instantaneous ideal measurements (projections) are performed at intervals τ, then $\rho_{ee}(t = n\tau) = \rho_{ee}^n(\tau)$. For a sufficiently large frequency of measurements $\nu \sim 1/\tau$, such that, at least, $\nu \gg \langle V^2\rangle^{1/2}/\hbar$, it follows from equation (2) that:

$$\rho_{ee}(t = n\tau) \approx \exp[-(\langle V^2\rangle\tau/\hbar^2)t] \tag{3}$$

Equation (3) may be limited to short times, such that $\rho_{ee}(t) \approx 1$, due to the possibility of transitions back from $|j\rangle$ to $|e\rangle$, which occurs, for example, when $|e\rangle$ is coupled to one[5–8] or more discrete states. However, when $|e\rangle$ is weakly coupled to a broad band of states (continuum), the transitions back to $|e\rangle$ can be neglected and equation (3) has no time restriction. As follows from equation (3), the decay rate of state $|e\rangle$ decreases with τ (the QZE), the evolution becoming frozen in the limit $\tau \to 0$, which is known as the quantum Zeno paradox[2–4]. The above argument seems compelling, and has led to the widespread opinion that the QZE is a necessary consequence of quantum mechanics, provided that the measurements performed on the system are ideal and sufficiently frequent (although a dissenting opinion has been voiced, based on a certain model of measuring the position of a tunnelling particle[11]).

As shown below, the energy uncertainty (spread) incurred by frequent ideal projections fundamentally restricts the QZE observability, and renders decay acceleration by frequent measurements far more ubiquitous than its inhibition. We refer to this universal effect (first discovered for spontaneous emission in cavities[12]) as the anti-Zeno effect (AZE). By contrast, a fundamental limitation on the observability of the QZE emerges from our theory: the intervals τ between consecutive measurements required for the QZE are so short for many processes (such as radiative and radioactive decay) that the resulting energy spread may destroy the observed system by coupling it to unwarranted channels—in the worst case, leading to the creation of new particles (for example, electron–positron pair creation by a spontaneously emitting atom).

To get deeper insight into the effect of frequent measurements, it is necessary to go beyond the standard expansion, equation (2). We write $\hat{H} = \hat{H}_0 + \hat{V}$, so that $|e\rangle$ is an eigenvector of $\hat{H}_0$ with the eigenvalue $\hbar\omega_a = \langle e|\hat{H}|e\rangle$, whereas $\hat{V}$ describes the interaction of $|e\rangle$ with other states, $\hat{V} = \Sigma_j(V_{ej}|e\rangle\langle j| + V_{je}|j\rangle\langle e|)$, where $V_{ej} = \langle e|\hat{H}|j\rangle$ and $\{|j\rangle\}$ is an arbitrary orthonormal basis of the subspace of the Hilbert space orthogonal to $|e\rangle$ (formally, $\hat{V} = [\hat{P}, [\hat{P}, \hat{H}]]$, where $\hat{P} = |e\rangle\langle e|$). Choosing $|j\rangle$ to be the eigenvectors of $\hat{H}_0$ with the eigenvalues $\hbar\omega_j$, we can write the wavefunction of the system as:

$$|\Psi(t)\rangle = \alpha(t)e^{-i\omega_a t}|e\rangle + \sum_j \beta_j e^{-i\omega_j t}|j\rangle \tag{4}$$

One can then obtain from the Schrödinger equation the following equations

$$\dot{\alpha} = -\frac{i}{\hbar}\sum_j V_{ej}e^{-i(\omega_a - \omega_j)t}\beta_j \tag{5}$$

$$\dot{\beta}_j = -\frac{i}{\hbar}V_{je}e^{-i(\omega_a - \omega_j)t}\alpha \tag{6}$$

the initial condition being $|\Psi(0)\rangle = |e\rangle$. Formally integrating equation (6) yields:

$$\beta_j(t) = -\frac{i}{\hbar}V_{je}\int_0^t dt' e^{-i(\omega_a - \omega_j)t'}\alpha(t') \tag{7}$$

Inserting equation (7) into equation (5), we obtain the exact integro-differential equation

$$\dot{\alpha} = -\int_0^t dt' e^{i\omega_a(t-t')}\Phi(t-t')\alpha(t') \tag{8}$$

where

$$\Phi(t) = \hbar^{-2}\sum_j |V_{ej}|^2 e^{-i\omega_j t} = \hbar^{-2}\langle e|\hat{V}e^{-i\hat{H}_0 t/\hbar}\hat{V}|e\rangle \tag{9}$$

Equation (8) is exactly soluble by the Laplace transform method. However, for the present study of frequent measurements it suffices to obtain the short-time behaviour, when $\alpha(t) \approx \alpha(0) = 1$. This can be done iteratively. Setting $\alpha(t') = 1$ on the right-hand side of equation (8) yields (after the first iteration):

$$\alpha(t) \simeq 1 - \int_0^t dt'(t-t')\Phi(t')e^{i\omega_a t'} \tag{10}$$

Note that as long as $\alpha(t) \approx 1$, powers of t higher than 2 can be important, even for $|V_{ej}|t \ll 1$, due to the exponent in equation (9), whence it follows that the standard expansion—equation (2)—may fail. Therefore the approximate result $\rho_{ee}(t) = |\alpha(t)|^2$, where $\alpha(t)$ is given by equation (10), is much more reliable than the commonly accepted[3,4,9,10] equation (2), as it takes into account all powers of t.

If instantaneous projections onto $|e\rangle$ are performed at sufficiently small intervals τ, we can write, using equation (10)

$$\rho_{ee}(t = n\tau) = |\alpha(\tau)|^{2n} \approx \exp(-Rt) \tag{11}$$

where the measurement-modified decay rate is given by:

$$R = 2\mathrm{Re}\int_0^\infty dt f(t)\Phi(t) \tag{12}$$

Here the measurement effects are accounted for by $f(t) = (1 - t/\tau)e^{i\omega_a t}\theta(\tau - t)$, where $\theta(x)$ is 1 for $x > 0$ and 0 for $x < 0$. The Fourier transform of $\Phi(t)$

$$G(\omega) = \frac{1}{\pi}\mathrm{Re}\int_0^\infty dt\Phi(t)e^{i\omega t} = \hbar^{-2}\sum_j |V_{ej}|^2\delta(\omega - \omega_j) \tag{13}$$

allows us to recast the expression for the measurement-modified decay rate (equation (12)) as

$$R = 2\pi\int_0^\infty d\omega G(\omega)F(\omega) \tag{14}$$

where

$$F(\omega) = \frac{\tau}{2\pi}\mathrm{sinc}^2\left(\frac{(\omega - \omega_a)\tau}{2}\right) \tag{15}$$

The function $G(\omega)$ in equation (13) is the spectral density of the states $|j\rangle$ weighted with the coupling strengths $\hbar^{-2}|V_{ej}|^2$. If the states $|j\rangle$ belong to a spectrally dense band ('reservoir'), $G(\omega) \to |V(\omega)|^2\rho(\omega)$, where $V(\omega)$ are the coupling constants to states $|\omega\rangle$, whose spectral density is given by $\rho(\omega)$. It is then called the reservoir coupling spectrum[13].

Whereas $G(\omega)$ is a property of the hamiltonian $\hat{H}$, the form factor $F(\omega)$ (equation (15)) shows the broadening (width) of ω_a, incurred by frequent measurements, to be of the order of the measurement frequency $\nu \sim 1/\tau$. Thus, equation (14) represents a universal result: the decay rate of a frequently measured state $|e\rangle$ is simply the overlap of the reservoir coupling spectrum and the measurement-induced level width (Fig. 1, upper inset, Fig. 2a).

Equation (14) shows that the decay rate is determined by the form of $G(\omega)$ in a band of width ν around ω_a. This can be interpreted as resulting from the broadening of level $|e\rangle$, in accordance with the energy–time uncertainty relation:

$$\Delta E\Delta t \sim \hbar \tag{16}$$

Here ΔE is the energy uncertainty of $|e\rangle$, equal to the characteristic width of $F(\omega)$ times $\hbar$, and $\Delta t = 1/\nu$ is the average interval between

the measurements. The effect of instantaneous measurements (projections) is to dephase level $|e\rangle$ (refs 4, 14), that is, make the phase of state $|e\rangle$ completely random. This effect is analogous to collisional broadening[13]: phase randomization by collisions yields a linewidth equal to the collision frequency ν_0, that is the same linewidth as in the case of an unstable state with lifetime $\Delta t = 1/\nu_0$.

A simple graphical analysis of equation (14) yields our three main conclusions.

(1) As shown in Fig. 1, upper inset, the QZE—that is, the reduction of the decay rate as the measurement (dephasing) rate ν increases—is generally obtained when the following inequalities are satisfied:

$$\nu \gg \Gamma_R, |\omega_a - \omega_M| \tag{17}$$

Here Γ_R is the reservoir width, and ω_M is the centre of gravity of $G(\omega)$. In this limit, we can make the approximation $G(\omega) \approx C\delta(\omega - \omega_M)$ in the integrand of R in equation (14), with $C = \int G(\omega)d\omega = \langle V^2 \rangle$. This approximation becomes exact in the case of resonant Rabi oscillations ($\Gamma_R = 0$, $\omega_a = \omega_M$), which explains why the QZE is observable in Cook's system for any ν (refs 5–8). More generally, this approximation holds for any $G(\omega)$ that falls off faster than $1/|\omega - \omega_M|$ on the wings. Then equation (14) yields the most general result for the QZE

$$R \approx 2C/\nu \tag{18}$$

where $1/\nu = \pi F(\omega_a)$. The flattening of the spectral peak of $G(\omega)$ by the broad function $F(\omega)$ in the convolution equation (14) (see Fig. 1, upper inset) is the origin of the QZE; that is, the reduction of R as compared to the measurement-free decay rate $\gamma_{free} = R(\nu \to 0) = 2\pi G(\omega_a)$, which is the 'golden rule' value[13]. To put it simply, if the system is probed frequently enough (as dictated by equation (17)), the QZE arises because the effective decay rate is averaged over all decay channels, many of which are weak, due to the energy uncertainty incurred by the measurements. The result, equation (18), is completely insensitive to the spectral shape of the reservoir: only its integral C matters (provided that equation (17) holds). The present analysis implies the possibility of inhibiting vibrational relaxation by the QZE in molecules and solids (Fig. 1).

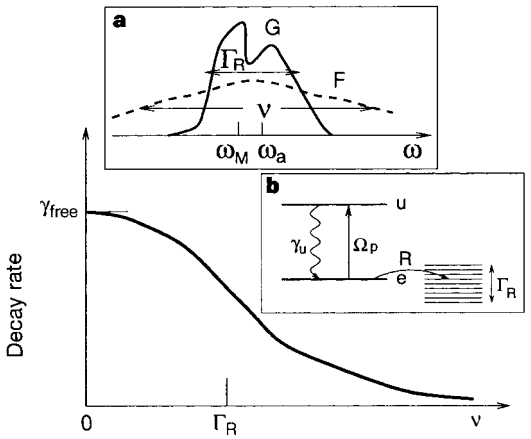

Figure 1 The QZE characteristics and a frequent-measurement scheme. Upper inset, conditions for the QZE (equation (17)) for a complicated reservoir-coupling spectrum $G(\omega)$ of width Γ_R (solid line) and measurement-induced level broadening $F(\omega)$ of width ν (dashed curve). Main figure, typical dependence of the decay rate R on ν under QZE conditions (equation (18)). Note that for decay near the cut-off frequency ω_c of a reservoir with $G(\omega) \propto (\omega_c - \omega)^{-\beta}$, where $0 < \beta < 1$ (for example, $\beta = 1/2$ for vibrational spectra with upper cut-off in molecules or solids), we find the QZE scaling to be slower, $R \propto \nu^{-\beta}$. Lower inset, scheme for frequent impulsive or continuous measurements of $|e\rangle$ (similar to refs 5,6,12).

(2) As shown in Fig. 2, left upper inset, the opposite behaviour is obtained in the limit

$$\nu \ll |\omega_m - \omega_a| \tag{19}$$

whenever ω_a is significantly detuned from the nearest maximum of $G(\omega)$ at ω_m, so that $G(\omega_a) \ll G(\omega_m)$. In this limit, the rate R grows with ν, because the dephasing fucntion $F(\omega)$ is then probing more of the rising part of $G(\omega)$ in the convolution, equation (14). Hence, this limit should always yield a scaling of R as a positive power of ν: that is, the anti-Zeno effect (AZE) of decay acceleration by frequent measurements. Physically this means that, as the energy uncertainty increases with the measurement rate ν, the state decays into more and more channels, whose weight $G(\omega)$ is progressively larger.

The present analysis reveals the universality of the AZE: we may impose condition of equation (19) in any reservoir, as seen from Fig. 2, left upper inset. Moreover, the AZE is inevitable in natural decay processes, such as the nuclear β-decay: in such processes, any measurement rate ν below the relativistic cut-off of the reservoir, $\nu \ll Mc^2/\hbar$ (where Mc^2 is the rest-mass energy of the decaying particle), would correspond in equation (14) to probing the rising reservoir response $G(\omega) \propto \omega^\eta$ with $\eta \geq 1$. The result for $\eta > 1$ is then the following AZE dependence of the decay rate:

$$R \propto \nu\omega_R^{\eta-1} \quad (\omega_a^\eta/\omega_R^{\eta-1} \ll \nu \ll \omega_R) \tag{20}$$

Higher measurement rates, $\nu \gtrsim \omega_R$, are not only unfeasible, but also detrimental to the system, leading to the production of new particles.

Similar considerations apply to a two-level system, consisting of an upper state $|e\rangle$ at energy $\hbar\omega_e$ and a lower state $|g\rangle$ at energy $\hbar\omega_g$, with state $|e\rangle$ coupled to a zero-temperature reservoir of harmonic oscillators. This description fits atomic radiative decay (spontaneous emission) into a vacuum field[13,15]. The effects of very frequent measurements, with $\nu \gtrsim \omega_a = \omega_e - \omega_g$, may be revealed in radiative decay of an excited hydrogenic (or Rydberg) level of a two-level

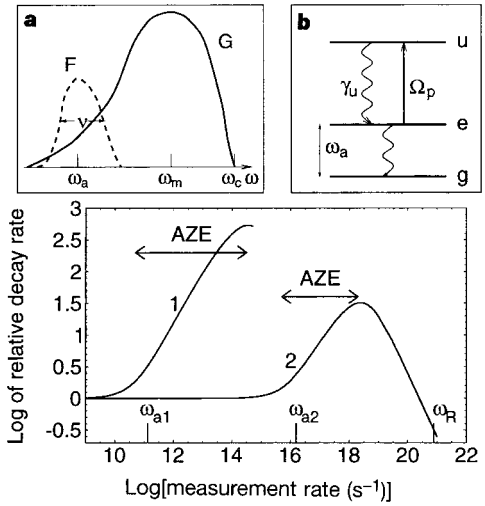

Figure 2 The AZE characteristics and a frequent-measurement scheme for two-level systems. **a**, Conditions for the AZE (equation (19)), with the same notation as in Fig. 1. Main figure, the dependence of the logarithm of the normalized decay rate $\log_{10}(R/\gamma_{free})$ on $\log_{10}\nu$ for a spontaneously emitting hydrogenic state. An exact calculation for this system[15] provides the reservoir-coupling spectrum $G(\omega) = \alpha\omega/[1 + (\omega/\omega_B)^2]^4$, where α is determined by the field-atom coupling strength and $\omega_B \sim c/a_B$ is the non-relativistic cut-off frequency, a_B being the radius of the electron orbit. Under condition of equation (19) we then obtain from equations (14) and (15) the following AZE dependence: $R = \alpha\nu[\ln(\omega_B/\nu) + 0.354](\omega_a \ll \nu \ll \omega_B)$, where $\nu = 2/\tau$. The vertical lines on the horizontal axis denote the values of the atomic transition frequencies corresponding to curves 1, 2: $\omega_{a1} = 1.32 \times 10^{11}\ s^{-1}$, $\omega_{a2} = 1.55 \times 10^{16}\ s^{-1}$, whereas $\omega_R = 7.76 \times 10^{20}\ s^{-1}$. The corresponding Bohr frequencies are $\omega_{B1} = 1.22 \times 10^{15}\ s^{-1}$, $\omega_{B2} = 8.50 \times 10^{18}\ s^{-1}$. The AZE ranges are marked. **b**, Scheme for realistic frequent measurements of the excited state in a two-level system[5,6,12].

system. As seen in Fig. 2, the AZE trend is revealed already for $\nu \lesssim \omega_a$, which should make its observation feasible, especially for microwave Rydberg transitions. A close inspection of Fig. 2 reveals that the decay rate R falls below the measurement-free (golden rule) decay rate γ_{free} only at $\nu \sim \omega_R$, which is not only unfeasible, but would imply a considerable probability of electron–positron pair creation. An additional limitation on the concept of measurement-influenced decay that is specific to two-level systems occurs for $\nu \gtrsim \omega_a$. The uncertainty of ω_a is then so large that occasionally $|g\rangle$ may be found at a higher energy than $|e\rangle$, which may cause $|g\rangle \rightarrow |e\rangle$ transitions. Such transitions are usually excluded by the rotating-wave approximation[13], which may fail in this case because of the large energy fluctuations caused by the frequent measurements. Under these conditions, equation (11) holds only at short enough times, $t \ll R^{-1}$, for which $|g\rangle$ is still unpopulated.

(3) We can retrieve the limit in which the decay rate is unaffected by measurements and is given by the golden rule: $R \rightarrow \gamma_{free} = 2\pi G(\omega_a)$. In the case of a continuous $G(\omega)$, this limit is obtained from equation (14) if the measurement rate (dephasing) ν is too small (typically, $\nu \ll \omega_a$) to probe the slope of the spectral response. It is tantamount to the Wigner–Weisskopf approximation[13] of purely markovian, exponential decay, $\rho_{ee}(t) \approx \exp(-\gamma_{free} t)$. This approximation is never strictly correct, because it requires an unphysical, spectrally flat reservoir $G(\omega) = \text{const.}\ (-\infty < \omega < \infty)$.

The arguments leading to equation (14) and the resulting effects have assumed ideal instantaneous projections on $|e\rangle$. Does a more realistic description of measurements still support these results? The answer is that their universality has been reaffirmed by detailed analysis of the two possible types of measurements of $|e\rangle$.

First, impulsive measurements[5,6,12,16]. Such measurements are realizable, for example, when the decay process is repeatedly interrupted by a short electromagnetic pulse transferring the population of $|e\rangle$ to a higher auxiliary state $|u\rangle$, which then decays back to $|e\rangle$ incoherently (Fig. 1, lower inset, and Fig. 2b). For such a measurement to qualify as impulsive, its duration, which is of the order of the decay time of the $|u\rangle$ state $1/\gamma_u$ (assuming that the $|e\rangle \rightarrow |u\rangle$ transfer is faster than this decay), must be negligible, that is, it must be much shorter than the interval between successive measurements τ, which in turn should be much shorter than the decay time of $|e\rangle$. The solution of the full master equations for these measurements conforms to equation (14) to a very good approximation[12,16], with the dephasing function given by equation (15).

Second, continuous measurements. These should not be confused with continuous observation identified[2] as the limit of vanishing intervals between successive projections ($\Delta t \rightarrow 0$ or $\nu \rightarrow \infty$). This limit is unphysical, corresponding to an infinite spread of energy fluctuations. Even finite, but excessively large ν, may be detrimental to the model, as argued above. In contrast, realistic continuous measurements, through monitoring the state incessantly, still require a finite time for completing an observation; that is, they have a finite effective rate ν. This can be illustrated by the case of stationary dephasing when the $|e\rangle \leftrightarrow |u\rangle$ transition is driven by a near-resonant continuous-wave field at a Rabi frequency Ω that is much smaller than the transition linewidth $\gamma_u/2$ (Fig. 1, lower inset, and Fig. 2, upper right inset). It can be shown that equation (14) holds for continuous measurements with $F(\omega)$ being a lorentzian centred at ω_a of width $\nu = 2\Omega^2/\gamma_u$.

We may infer from the above discussion that, qualitatively, in all the cases considered above there is no essential distinction between different frequent measurements: ideal projections, impulsive measurements, and continuous measurements. We also note that, as the effect of both the impulsive and continuous measurements is tantamount to the dephasing of $|e\rangle$ at a rate ν, it is possible to mimic their effect by a stochastic (fluctuating) broadband field[17]. In all cases of realistic measurements, the spectral width ν of measurement-induced dephasing can be attributed to the time–energy uncertainty.

The simple criteria obtained from the universal formula, equation (14), lead us to conclude that the QZE—that is, decay inhibition by frequent measurements, whether ideal or more realistic—is strictly attainable only for decay into narrow reservoirs, whose spectral width is below the energy of the decaying state. This is the reason why the QZE is observable for Rabi oscillations[5–8], and is predicted here to be feasible for vibrational decay in molecules or solids (Fig. 2). Yet the QZE concept is untenable whenever the required broadening of the level by frequent measurements is so large that it has spectral overlap with transitions from the decaying state $|e\rangle$ to states outside the original reservoir. In particular, the QZE is incompatible with processes, such as the nuclear β-decay or spontaneous emission, wherein the reservoir response $G(\omega)$ grows with frequency almost up to the relativistic cut-off ω_R. The QZE requirement is then $\nu \gtrsim \omega_R$, and may result in the production of new particles (or other unwarranted effects specific to spontaneous emission, due to the breakdown of the rotating-wave approximation) and thus must be ruled out. By contrast, the condition of equation (19) for the accelerated decay (AZE) trend is in principle realizable for decay into any reservoir, whether spectrally broad or narrow, and is therefore far more ubiquitous than the QZE. This surprising conclusion can be experimentally tested: we predict that accelerated radiative decay is achievable for microwave transitions, $\omega_a \lesssim 10^{11}\ s^{-1}$, in Rydberg atoms perturbed by randomizing collisions with a buffer gas at a rate $\nu \sim \omega_a$ or a fluctuating field with bandwidth $\nu_f \gtrsim \omega_a$ (Fig. 2). Another prediction is AZE for β-decay, according to equations (19) and (20), which may be achievable by perturbing the decaying nuclear state with a broadband (fluctuating) γ-ray source. Thus the present findings may serve as clues to our ability to manipulate diverse decay processes.

The essential restrictions on the QZE observability found here evoke one of Zeno's paradoxes (the 'Achilles') that has not been discussed in the context of quantum mechanics. This paradox arises if we assume that time is divisible *ad infinitum*. In this paradox, the running Achilles can never catch the crawling tortoise in front of him, because he must first reach where the tortoise started. But when he reaches there, the tortoise has moved ahead, and so on. Quantum measurement theory supports Zeno's reservations regarding infinitesimal time intervals, because they exact an impossible toll: energy spread tending to infinity (according to the time–energy uncertainty relation), with detrimental consequences to the system below a certain minimal time interval. □

Received 26 August 1999; accepted 8 March 2000.

1. Khalfin, L. S. Phenomenological theory of K^0 mesons and the non-exponential character of the decay. *JETP Lett.* **8,** 65–68 (1968).
2. Misra, B. & Sudarshan, E. C. G. The Zeno's paradox in quantum theory. *J. Math. Phys.* **18,** 756–763 (1977).
3. Sakurai, J. J. *Modern Quantum Mechanics* 484–486 (Addison-Wesley, Reading, Massachusetts, 1994).
4. Joos, E. Continuous measurement: Watchdog effect versus golden rule. *Phys. Rev. A* **29,** 1626–1633 (1984).
5. Cook, R. J. What are quantum jumps? *Phys. Scr. T* **21,** 49–51 (1988).
6. Itano, W. M., Heinzen, D. J., Bollinger, J. J. & Wineland, D. J. Quantum Zeno effect. *Phys. Rev. A* **41,** 2295–2300 (1990).
7. Knight, P. L. Watching a laser hot-pot. *Nature* **344,** 493–494 (1990).
8. Frerichs, V. & Schenzle, A. Quantum Zeno effect without collapse of wave packet. *Phys. Rev. A* **44,** 1962–1968 (1991).
9. Schulman, L. S. Continuous and pulsed observations in the quantum Zeno effect. *Phys. Rev. A* **57,** 1509–1515 (1998).
10. Facchi, P. & Pascazio, S. Temporal behavior and quantum Zeno time of an excited state of the hydrogen atom. *Phys. Lett. A* **241,** 139–144 (1998).
11. Fearn, H. & Lamb, W. E. Jr Computational approach to the quantum Zeno effect: Position measurements. *Phys. Rev. A* **46,** 1199–1205 (1992).
12. Kofman, A. G. & Kurizki, G. Quantum Zeno effect on atomic excitation decay in resonators. *Phys. Rev. A* **54,** R3750–R3753 (1996).
13. Cohen-Tannoudji, C., Dupont-Roc, J. & Grynberg, G. *Atom-Photon Interactions* (Wiley, New York, 1992).
14. Milburn, G. J. Quantum Zeno effect and motional narrowing in a two-level system. *J. Opt. Soc. Am. B* **5,** 1317–1322 (1988).
15. Moses, H. E. Exact electromagnetic matrix elements and exact selection rules for hydrogenic atoms. *Lett. Nuovo Cimento.* **4,** 51–53 (1972).
16. Beige, A. & Hegerfeldt, G. C. Quantum Zeno effect and light-dark periods for a single atom. *J. Phys. A* **40,** 1323–1334 (1997).

17. Harel, G., Kofman, A. G., Kozhekin, A. & Kurizki, G. Control of non-Markovian decay and decoherence by measurements and interference. *Opt. Express* **2,** 355–367 (1998).

Acknowledgements

G.K. is the G. Dunne Professor of Chemical Physics, A.K. is supported by the Israel Ministry of Absorption. This work was supported by the ISF, Minerva and EU (TMR).

Correspondence and requests for materials should be addressed to G.K. (e-mail: Gershon.Kurizki@weizmann.ac.il).

Absence of thermodynamic phase transition in a model glass former

Ludger Santen & Werner Krauth

CNRS-Laboratoire de Physique Statistique, Ecole Normale Supérieure, 24 rue Lhomond, 75231 Paris Cedex 05, France

The glass transition can be viewed simply as the point at which the viscosity of a structurally disordered liquid reaches a universal threshold value[1]. But this is an operational definition that circumvents fundamental issues, such as whether the glass transition is a purely dynamical phenomenon[2]. If so, ergodicity gets broken (the system becomes confined to some part of its phase space), but the thermodynamic properties of the liquid remain unchanged across the transition, provided they are determined as thermodynamic equilibrium averages over the whole phase space. The opposite view[3–6] claims that an underlying thermodynamic phase transition is responsible for the pronounced slow-down in the dynamics at the liquid–glass boundary. Such a phase transition would trigger the dynamic standstill, and then be masked by it. Here we perform Monte Carlo simulations of a two-dimensional system of polydisperse hard disks far within its glassy phase. The approach[7] allows for non-local moves in a way that preserves micro-reversibility. We find no evidence for a thermodynamic phase transition up to very high densities; the glass is thus indistinguishable from the liquid on purely thermodynamic grounds.

We considered polydisperse hard disks $i = 1, \ldots, N$ with radii r_i (where $r_i - r_{i-1} = \Delta/(N-1)$) in a square box of volume $V = L^2$ with periodic boundary conditions. The polydispersity Δ/r_1 was kept fixed and the system was studied as a function of the density $\rho = \pi\Sigma_i r_i^2/L^2$. We note that hard-core systems are athermal: the phase diagram and the dynamics (up to a trivial rescaling) are independent of temperature. The external control parameters are the density (for the [NV] ensemble) or the pressure (for [NP]).

Conventional, local-move Monte Carlo simulations in the [NV] ensemble were used to compute effective diffusion constants[8] at densities for which the local algorithm was still ergodic (Fig. 1). We failed to detect any finite-size effects by comparing runs with 256 and 1024 disks at density $\rho = 0.764$, but we noticed strong dependence of the diffusivities on the disk size. For each disk i we found its diffusivity D_i to agree very well with[9]

$$D_i(\rho) \approx (\rho - \rho_i^G)^\alpha \qquad (1)$$

For the 180 largest disks we found no systematic dependence of $\rho_i^G = \rho^G \cong 0.805 \pm 0.01$ (with a best fit $\alpha \approx 2.4$). For the smallest disks i, the extrapolated values for ρ_i^G increased slowly. Our result for ρ^G agrees with what was found in a related system[10].

We next performed simulations with the cluster Monte Carlo algorithm[7]. There, groups of disks are swapped around a 'pivot' in a way which represents an alternative Markov-chain sampling of the Boltzmann distribution. The correctness of both implementations was validated by comparing structural quantities (pair correlation functions) and thermodynamic variables in the manifestly liquid regime, where the local algorithm still converges well. We found that the cluster Monte Carlo algorithm does not slow down as we pass ρ_G.

We used the cluster Monte Carlo algorithm to compute the equation of state in the [NP] ensemble[8]. For pressures corresponding to the glass transition density ρ^G, we reached a relative precision for V of 0.05% during a one-week simulation on a single processor workstation ($N = 256$). The compressibility of the system was obtained both by deriving the algebraic fit to $V(P)$ (see Fig. 2

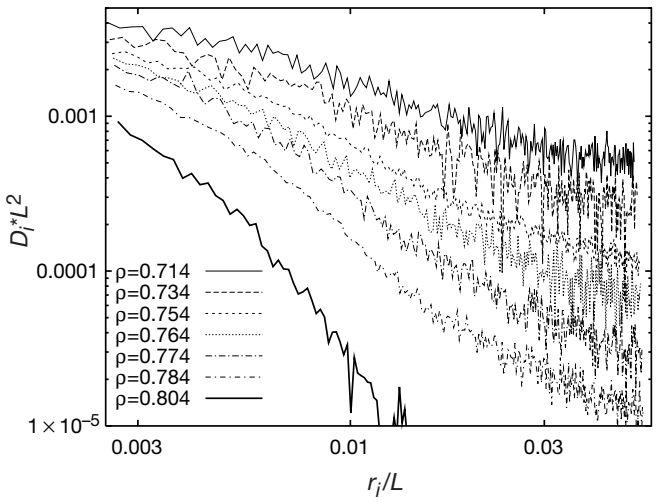

Figure 1 Effective diffusion constants as a function of the radius for polydisperse hard disks. The upper 6 curves represent 256 disks with polydispersity $\Delta/r_1 = 19$ simulated using the local-move Monte Carlo algorithm at densities for which the algorithm equilibrated. The effective diffusion constants were calculated using $D_i = \langle(\mathbf{x_i}(t_0 + t) - \mathbf{x_i}(t_0))^2\rangle/(4t)$, for $|\mathbf{x_i}(t_0 + t) - \mathbf{x_i}(t_0)| \gg r_N$. The time was measured in Monte Carlo sweeps. Only the motion relative to the largest disk was taken into account. These asymptotic constants agree (up to a rescaling of the time unit) with what would be obtained in a molecular dynamics simulation[8]. The lowest curve is as above, but equilibrated initial configurations were provided by the cluster Monte Carlo algorithm. We observe that the smallest 50 disks are able to pass through the blocked matrix made up of the largest 200 disks. These findings are consistent with the estimated values of the transition densities. L, side of box containing disk. r_i, radius of disk i.

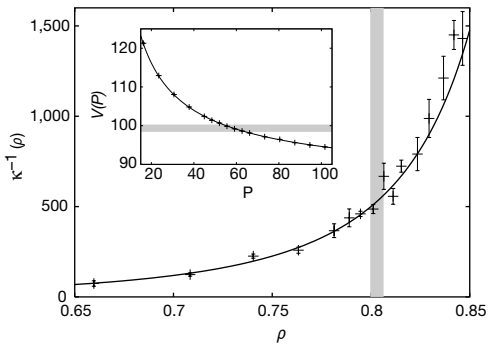

Figure 2 Equilibrium compressibility. The system, as before, was simulated using the cluster Monte Carlo algorithm. The equilibrium equation of state (inset) and inverse compressibility κ^{-1} (main figure) were obtained in the [NP] ensemble. κ was obtained from the fluctuations of the volume (points with error bars) and from the derivative of the best $V(P)$ fit according to the functional form $V(P) - k = aP^{-b}$ (k is a constant; the parameters of the best fit are $k = 84.3$, $a = 254$, $b = 0.69$). Indications of an equilibrium phase transition are lacking. The grey lines indicate the localization of the glass transition as extrapolated from Fig. 1.